

## Multiple minimum-energy paths and scenarios of unwinding transitions in chiral nematic liquid crystals

Semen S. Tenishchev <sup>1,2,\*</sup> Alexei D. Kiselev <sup>1,2,†</sup> Aleksei V. Ivanov<sup>2,3,‡</sup> and Valery M. Uzdin <sup>2,1,§</sup>

<sup>1</sup>*Department of Mathematics, ITMO University, Kronverkskiy, 49, 197101 Saint Petersburg, Russia*

<sup>2</sup>*Faculty of Physics, Saint Petersburg State University, 199034 Saint Petersburg, Russia*

<sup>3</sup>*Science Institute and Faculty of Physical Sciences, University of Iceland VR-III, 107 Reykjavík, Iceland*



(Received 10 November 2019; published 31 December 2019)

We apply the minimum-energy paths (MEPs) approach to study the helix unwinding transition in chiral nematic liquid crystals. A mechanism of the transition is determined by a MEP passing through a first order saddle point on the free energy surface. The energy difference between the saddle point and the initial state gives the energy barrier of the transition. Two starting approximations for the paths are used to find the MEPs representing different transition scenarios: (a) the director slippage approximation with in-plane helical structures and (b) the anchoring breaking approximation that involves the structures with profound out-of-plane director deviations. It is shown that, at sufficiently low voltages, the unwinding transition is solely governed by the director slippage mechanism with the planar saddle-point structures. When the applied voltage exceeds its critical value below the threshold of the Fréedericksz transition, the additional scenario through the anchoring breaking transitions is found to come into play. For these transitions, the saddle-point structure is characterized by out-of-plane deformations localized near the bounding surface. The energy barriers for different paths of transitions are computed as a function of the voltage and the anchoring energy strengths.

DOI: [10.1103/PhysRevE.100.062704](https://doi.org/10.1103/PhysRevE.100.062704)

### I. INTRODUCTION

Helical superstructures naturally arise in certain liquids with long-range orientational order characterizing the liquid crystalline (mesomorphic) state that occurs in a temperature range between the liquid and the solid (crystalline) phases. In these orientationally ordered liquids known as the *liquid crystals* (LCs) the molecules tend to align along a preferred direction typically described in terms of the LC director which is a unit vector  $\hat{\mathbf{n}}(\mathbf{r})$  representing the locally averaged direction of the LC molecules at a point  $\mathbf{r}$  in the liquid crystalline material [1,2]. It is the presence of the LC orientational order that leads to an optical and electromagnetic anisotropy which has been extensively exploited in the nowadays widespread liquid crystal technology [3,4].

Helical twisting patterns where the director rotates in a helical fashion about a uniform twist (helical) axis spontaneously form in unbounded chiral liquid crystals and are caused by the presence of anisotropic molecules with no mirror plane—the so-called chiral molecules. These patterns thus represent self-organized soft helical superstructures.

The supramolecular helical architectures are at the heart of a unique combination of photonic properties of chiral nematic liquid crystals, otherwise referred to as the *cholesteric liquid crystals* (CLCs).

LCs are known to be responsive materials that are highly sensitive to external stimuli such as electromagnetic fields and

boundary (anchoring) conditions. This responsiveness underpins tunability of the helical structures underlying most of the fascinating device applications of CLCs and controllable manipulation of the CLC helical superstructures presents a challenging problem which is of vital importance for both fundamental and technological reasons [5–8].

An ideal CLC helix is specified by orientation of the twisting axis,  $\hat{\mathbf{h}}$ , and the *helix pitch*,  $P$ , that also govern its optical properties. In planar confining geometry of typical CLC cells, where the CLC is sandwiched between two parallel bounding surfaces (substrates), the planar Grandjean structure (texture) which is the uniform standing helix state with the helical axis  $\hat{\mathbf{h}} = \hat{\mathbf{z}}$  normal to the substrates

$$\hat{\mathbf{n}} = \cos \phi \hat{\mathbf{x}} + \sin \phi \hat{\mathbf{y}}, \quad \phi = qz + \phi_0, \quad (1)$$

where  $q = \pm 2\pi/P$  is the *helix wave number* which is positive (negative) for the right-handed (left-handed) helix and exemplifies the special case of anisotropic one-dimensional photonic crystals. It is characterized by a chirally sensitive photonic band gap. Circularly polarized light with helicity identical to the handedness of the helix cannot propagate, and selective reflection takes place.

The well-established continuum theory describing the phenomenology of CLCs is formulated in terms of the Frank-Oseen free energy functional  $F_{\text{el}}[\mathbf{n}]$  and the elastic free energy density  $f_{\text{el}}$  [9,10]:

$$F_{\text{el}}[\mathbf{n}] = \int_V f_{\text{el}} dv, \quad f_{\text{el}} = \frac{1}{2} \{ K_1 (\nabla \cdot \mathbf{n})^2 + K_2 [\mathbf{n} \cdot \nabla \times \mathbf{n} + q_0]^2 + K_3 [\mathbf{n} \times (\nabla \times \mathbf{n})]^2 - K_{24} \text{div}[\mathbf{n} \text{div} \mathbf{n} + \mathbf{n} \times (\nabla \times \mathbf{n})] \}, \quad (2)$$

\*tenishchev.semen@gmail.com

†alexei.d.kiselev@gmail.com

‡alxvov@gmail.com

§v\_uzdin@mail.ru

where  $K_1$ ,  $K_2$ ,  $K_3$ , and  $K_{24}$  are the splay, twist, bend, and saddle-splay Frank elastic constants. As a manifestation of the chirality caused by the broken mirror symmetry the expression for the bulk free energy (2) contains a chiral term proportional to the free twist wave number  $q_0$  that gives the pitch  $P_0 \equiv 2\pi/|q_0|$  of equilibrium helical structures in unbounded CLCs.

An efficient method widely used to prepare CLCs is doping nematic LC mixtures with chiral additives that induce a helical structure [2,8]. For photosensitive chiral dopants (photoswitches), their helical twisting power and thus the CLC equilibrium helix pitch  $P_0$  can be controlled by light through photoinduced changes in chiral molecular switch conformation that influence the LC's helical twisting power [11–18]. Phototunability of the helix pitch leads to a variety of technologically promising effects such as the phototunable selective reflection, i.e., a light-induced change in the spectral position of the band gap [19–22].

An important point is that director configurations in the planar CLC cells are strongly affected by the anchoring conditions at the substrates. These conditions break the translational symmetry along the twisting axis and, in general, the helical form of the director field will be distorted. Nevertheless, when the anchoring conditions are planar and out-of-plane deviations of the director are suppressed, it might be expected that the configurations still have the form of the ideal helical structure (1). But, by contrast with the case of unbounded CLCs, the helix twist wave number  $q$  will now differ from  $q_0$ .

A mismatch between the twist imposed by the boundary conditions and the equilibrium pitch  $P_0$  may produce two metastable twist states that are degenerate in energy and can be switched either way by applying an electric field [23]. More generally metastable twist states in CLC cells appear as a result of competing influences of the bulk and the surface contributions to the free energy leading to frustration [2,24] and giving rise to multiple local minima of the energy [25] (results on multiple equilibria of LCs confined in the two-dimensional geometry of square domains were reported in Ref. [26]). Properties of the metastable helical structures are determined by the free twisting number  $q_0$  and the anchoring energy. Variations in  $q_0$  will affect the twisting wave number,  $q$ , and may result in sharp transitions—the so-called pitch transitions—between different branches of metastable states.

In particular, these transitions manifest themselves in a jumplike temperature dependence of selective light transmission spectra [27–30]. Different mechanisms behind the temperature variations of the pitch in CLC cells and hysteresis phenomena were discussed in Refs. [31–33]. A comprehensive stability analysis of the planar helical structures in CLC cells with symmetric and asymmetric boundary conditions was performed in Ref. [34]. The effects of bistable surface anchoring and mechanical strain on the pitch transitions have been studied theoretically in the recent papers [35] and [36,37], respectively. Results on light-induced dynamics of the pitch transitions in photosensitive CLCs were reported in Refs. [15,38]. The photoresponsive substrates can also be used as aligning surfaces with the anchoring conditions driven by light that result in surface mediated orientational dynamics [39–41].

Another standard and widely exploited technique to manipulate the helical structures uses their sensitivity to external (magnetic or electric) fields applied to CLC cells. An external field will generally distort the free energy landscape. These distortions lead to a variety of field-induced orientational effects such as the Fréedericksz and unwinding transitions that have attracted considerable attention in the context of electro-optics of LC display devices.

In the technologically important geometry where the electric field is applied across the CLC cell, these effects crucially depend on a number of factors such as the cell thickness  $L$ , the pitch  $P_0$ , the applied voltage  $U$ , the anchoring conditions, and elastic and dielectric properties of the CLC material [23,42–48]. In this geometry, the CLC cell with planar (homogeneous) anchoring conditions is subjected to the field applied along the twisting axis of the planar helical structure (1). This is the case of our primary concern.

The purpose of this paper is to explore global properties of the free energy landscape related to transitions between CLC states which are local minima (minimizers) of the free energy. The free energy pathways connecting pairs of metastable helical states appear as basic elements of a natural mathematical language dealing with the relevant geometry of the landscape viewed as a multidimensional free energy surface [49–51].

The key elements associated with the transitions are the *minimum-energy paths* (MEPs) between the initial and final states on the free energy surface. Every point on such a pathway is a free energy minimum in all but a certain direction in the configuration space of CLC director structures. The maximum along the MEP determines the *transition state* which is a saddle point on the free energy surface. The MEP itself represents a path with the maximal statistical weight and defines a scenario of the most probable transition between the states. The energy barrier separating the states can be found as the difference between the saddle-point energy and the energy of the initial state. When the transition goes through several metastable states, the MEP gives a sequence of the barriers to be passed in the course of the transition.

Information about such energy barriers is required to assess the effect of thermally activated transitions within the framework of the rate theory [52,53]. Similarly, in Refs. [54,55], the barrier heights and the Arrhenius formula were employed to estimate the rate of transitions between metastable twist states and the effective intrinsic torsional viscosity of LC cells with strong anchoring conditions.

In this paper we restrict our analysis to the case where stability of the CLC helix is determined by the threshold voltages of the Fréedericksz transition and apply the geodesic nudged elastic band (GNEB) method [50] to calculate MEPs of the helix unwinding transition between a metastable CLC twist state and the untwisted ground state. From the computed MEPs we identify two different scenarios for unwinding of the CLC helix to occur. These are (a) the transitions dominated by in-plane director slippage and (b) the transitions involving localized anchoring breaking. We shall study how these transitions and their free energy barriers depend on the electric field and the anchoring conditions.

The layout of the paper is as follows. General relations that determine the characteristics of the helical structures in CLC cells are given in Sec. II. Then in Sec. III we outline

the numerical procedure that we employ to compute MEPs and describe the results obtained using the director slippage and anchoring breaking approximations as starting approximations for the MEPs. Finally, in Sec. IV we discuss our results and make some concluding remarks.

## II. FREE ENERGY

We consider a CLC cell of thickness  $L$  sandwiched between two parallel plates that are normal to the  $z$  axis:  $z = -L/2$  (lower substrate) and  $z = L/2$  (upper substrate). Anchoring conditions at both substrates are planar (homogeneous) with the preferred orientation of CLC molecules at the lower and upper plates defined by the two vectors of easy orientation:  $\hat{\mathbf{e}}_-$  and  $\hat{\mathbf{e}}_+$ , where a hat will indicate unit vectors. These vectors are given by

$$\hat{\mathbf{e}}_{\pm} = \cos \psi_{\pm} \hat{\mathbf{x}} + \sin \psi_{\pm} \hat{\mathbf{y}}. \quad (3)$$

Then  $\Delta\psi = \psi_+ - \psi_-$  is the twist angle imposed by the boundary conditions.

We shall also write the CLC free energy functional as a sum of the bulk and surface contributions

$$F[\mathbf{n}, \mathbf{E}] = F_b[\mathbf{n}, \mathbf{E}] + F_s[\mathbf{n}], \quad (4)$$

$$F_s[\mathbf{n}] = \sum_{\nu=\pm 1} \int_{z=\nu L/2} W_{\nu}(\mathbf{n}) ds,$$

where  $\mathbf{E}$  is the electric field, and assume that both the polar and the azimuthal contributions to the anchoring energy  $W_{\nu}(\mathbf{n})$  can be taken in the form of the Rapini-Papoular potential [56]:

$$W_{\nu}(\mathbf{n}) = \frac{W_{\phi}^{(\nu)}}{2} [1 - (\mathbf{n} \cdot \hat{\mathbf{e}}_{\nu})^2]_{z=\nu L/2} + \frac{W_{\theta}^{(\nu)} - W_{\phi}^{(\nu)}}{2} (\mathbf{n} \cdot \hat{\mathbf{z}})^2_{z=\nu L/2}, \quad (5)$$

where  $W_{\phi}^{(+)}$  ( $W_{\phi}^{(-)}$ ) and  $W_{\theta}^{(+)}$  ( $W_{\theta}^{(-)}$ ) are the azimuthal and the polar anchoring strengths at the upper (lower) substrate.

Then we express the CLC director  $\mathbf{n}$  in terms of the polar and the azimuthal angles,  $\theta$  and  $\phi$ , as follows:

$$\mathbf{n} = \sin \theta \cos \phi \hat{\mathbf{x}} + \sin \theta \sin \phi \hat{\mathbf{y}} + \cos \theta \hat{\mathbf{z}}, \quad (6)$$

where the angles are functions of  $z$ ,  $\theta = \theta(z)$ , and  $\phi = \phi(z)$ , provided invariance with respect to in-plane translations is unbroken. After substituting the director parametrization (6) into Eq. (5), we have the surface potential in the following form:

$$F_s[\mathbf{n}]/A = \sum_{\nu=\pm 1} \left[ \frac{W_{\phi}^{(\nu)}}{2} \sin^2 \theta_{\nu} \sin^2(\phi_{\nu} - \psi_{\nu}) + \frac{W_{\theta}^{(\nu)}}{2} \cos^2 \theta_{\nu} \right], \quad (7)$$

where  $A$  is the area of the substrates,  $\theta_{\nu} \equiv \theta(\nu L/2)$ , and  $\phi_{\nu} \equiv \phi(\nu L/2)$ .

The bulk part of the free energy functional (4)

$$F_b[\mathbf{n}, \mathbf{E}] = F_{el}[\mathbf{n}] + F_E[\mathbf{n}, \mathbf{E}] \quad (8)$$

is a sum of the Frank-Oseen elastic energy  $F_{el}[\mathbf{n}]$  given by Eq. (2) and the electrostatic energy of interaction between the

electric field  $\mathbf{E}$  and CLC molecules,  $F_E[\mathbf{n}, \mathbf{E}]$ . For the CLC director (6), the elastic energy (2) takes the following form:

$$F_{el}[\mathbf{n}]/A = \frac{1}{2} \int_{-L/2}^{L/2} \{K_1(\theta)[\theta']^2 + K_2(\theta) \sin^2 \theta [\phi']^2 - 2C(\theta)\phi'\} dz, \quad (9)$$

$$K_i(\theta) = K_i \sin^2 \theta + K_3 \cos^2 \theta, \quad C(\theta) = q_0 K_2 \sin^2 \theta, \quad (10)$$

where the prime symbol stands for the derivative with respect to  $z$ .

In our case, the electric field is normal to the substrates  $\mathbf{E} = E_z(z)\hat{\mathbf{z}}$  with  $E_z(z) = -V'(z)$ , where  $V(z)$  is the electrostatic potential. It meets the Maxwell equation:  $\text{div } \mathbf{D} = 0$  for the electric displacement  $\mathbf{D} = \boldsymbol{\epsilon} \mathbf{E}$  linearly related to  $\mathbf{E}$  through the uniaxially anisotropic dielectric tensor  $\boldsymbol{\epsilon}$  with the components

$$\epsilon_{ij} = \epsilon_{\perp} \delta_{ij} + \epsilon_a n_i n_j, \quad \epsilon_a = \epsilon_{\parallel} - \epsilon_{\perp}, \quad (11)$$

where  $\delta_{ij}$  is the Kronecker symbol and  $i, j \in \{x, y, z\}$ ;  $\epsilon_{\perp}$  and  $\epsilon_{\parallel}$  are the dielectric constants giving the principal values of  $\boldsymbol{\epsilon}$ . So, the normal component of  $\mathbf{D}$ ,  $D_z = \epsilon_{zz} E_z$ , is independent of  $z$  and we obtain the relation linking the voltage applied across the CLC and  $D_z$ :

$$U = V(-L/2) - V(L/2) = \int_{-L/2}^{L/2} E_z dz = D_z \int_{-L/2}^{L/2} \frac{dz}{\epsilon_{zz}(\theta)}, \quad (12)$$

where  $\epsilon_{zz}(\theta) = \epsilon_{\perp} + \epsilon_a \cos^2 \theta$ . When the applied voltage is fixed, the electrostatic part of the energy

$$F_E = -\frac{1}{2} \int_V (\mathbf{E} \cdot \mathbf{D}) dv \quad (13)$$

assumes the form of a nonlocal functional:

$$F_E/A = -\frac{U^2}{2E[\theta]}, \quad E[\theta] = \int_{-L/2}^{L/2} \frac{dz}{\epsilon_{zz}(\theta)}. \quad (14)$$

In our subsequent calculations, we shall use the Frank elastic constants typical for 5CB [57]— $K_1 = 4.5$  pN,  $K_2 = 3.0$  pN, and  $K_3 = 6.0$  pN—and consider the case of the weakly twisted symmetric CLC cell of the thickness  $L = 5 \mu\text{m}$  with  $q_0 L = 0.05$ ,  $W_{\phi}^{(\pm)} \equiv W_{\phi} = 0.05$  mJ/m<sup>2</sup>, and  $\hat{\mathbf{e}}_{\pm} = \hat{\mathbf{x}}$ . These parameters are used to obtain the estimates we briefly discuss below.

In the absence of an electric field, the field free planar CLC helical structures (1) can be analyzed using the results of Ref. [34]. According to this analysis, the transitions of our primary concern involve three (meta)stable structures shown in Fig. 1: (a) the left-handed twisted structure with  $qL \approx -3.066$ , (b) the right-handed twisted structure with  $qL \approx 3.069$ , and (c) the nearly untwisted (nematic) structure with  $qL \approx 0.001$ . Since the free twist parameter  $q_0 L$  is small, the twisted structures are nearly degenerate in energy. The nematic structure is the stable state with the lowest energy (the energy difference per unit area can be estimated at about  $3.0 \mu\text{J}/\text{m}^2$ ).

The threshold voltage of the Fréedericksz transition  $U_{th}$  can be estimated using the analytical relations derived in Ref. [48]:

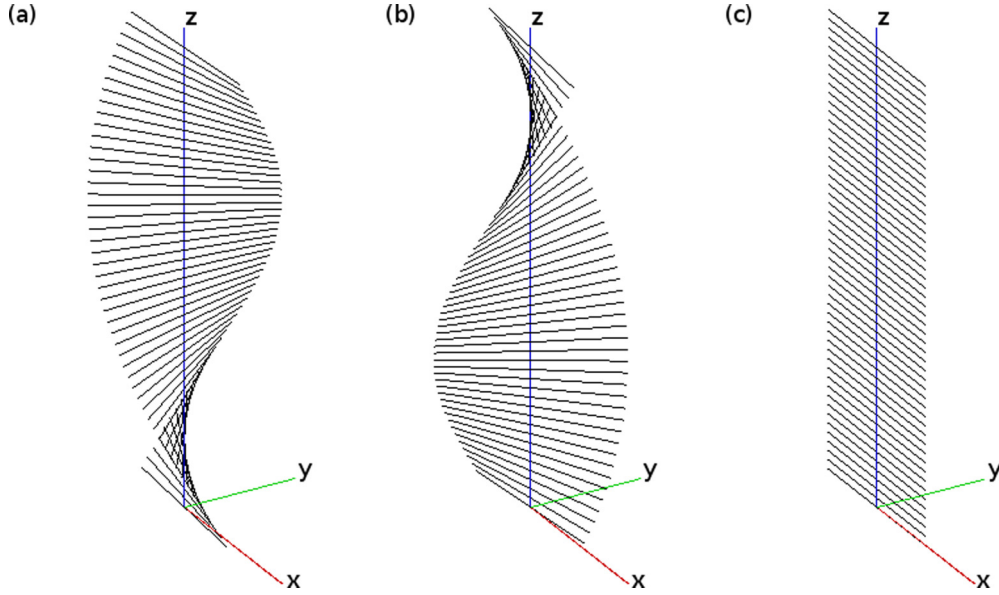


FIG. 1. Field free states: (a) the metastable left-handed helical (twisted) structure; (b) the metastable right-handed helical (twisted) structure; (c) the stable untwisted (nematic) structure.

$U_{\text{th}} \approx 0.578$  V. These relations also predict that, in our case, the transition leading to instability of the ground state will be continuous.

### III. RESULTS

In this section, we will focus on the unwinding transition from the metastable left-handed helix state to the stable nematic (equilibrium) state (see Fig. 1). Such a situation may occur in the light-induced pitch transitions in CLCs doped with photosensitive chiral dopants [15] when under the action of irradiation the free twisting number  $q_0$  changes from the initial value close to  $-\pi/L$  to the value close to zero.

The states differ in the parity of half turns [34] and are thus topologically distinct. The latter implies that, in the strong anchoring limit, the helical state cannot be smoothly deformed into the untwisted state without destroying the local degree of molecular ordering. By contrast, in the weak anchoring regime where the anchoring strength  $W_\phi$  is not infinitely large, these states are local minima of the multidimensional free energy surface separated by the finite energy barriers. We shall apply the minimum-energy path approach to study how these barriers are affected by the applied electric voltage  $U$  and the anchoring strength ratio  $r_{\text{orw}} = W_\theta/W_\phi$ , where  $W_\theta = W_\theta^\pm$ . After brief discussion of our method, we present the results for two classes of the pathways representing the two different scenarios of the unwinding transition: The *director slippage transitions* where the out-of-plane deviations of the director are suppressed ( $\theta \approx \pi/2$ ) and the *anchoring breaking transitions* that involve the states characterized by profound variations in the polar angle  $\theta$ .

#### A. Minimum-energy paths

In our calculations, the cell is divided into 100 equidistant layers and the director orientation is assumed to be constant inside each layer. Since the director in each layer has two

degrees of freedom (the azimuthal and the polar angles), the dimension of the free energy surface equals twice the number of the layers. This surface can be regarded as a 200-dimensional Riemannian manifold defined as a direct product of 100 two-dimensional spheres.

As in Ref. [51], we have used the GNEB method to find MEPs between local minima on the curved manifolds [50]. This approach involves taking an initial guess of a path between the two minima and systematically bringing that to the nearest MEP. A path is represented by a discrete chain of states, or “images,” of the system, where the first and the last image are placed at the local energy minima corresponding to the initial and final metastable configurations. In order to distribute the images evenly along the path, springs are introduced between adjacent images. At each image, a local tangent to the path needs to be estimated, and the force guiding the images towards the nearest MEP is defined as the sum of the transverse component of the energy antigradient plus the component of the spring force along the tangent to the path. The position of intermediate images is then adjusted so as to zero the GNEB forces.

An important point is that the MEP connecting the metastable structures generally depends on the starting approximation for the path. Variations in the initial approximations may produce different MEPs. Such paths represent distinct scenarios of the transition. Therefore, we have used different initial paths in order to study the two scenarios of the unwinding transition.

To find the director distributions for the initial and final states that should be solutions of the stationary point boundary problem (the Euler-Lagrange equations with the corresponding boundary conditions) we have started from the initial approximation for the director structure and then minimized the energy using the velocity projection algorithm [58]. The position of the maximum (saddle point) along the MEP was found using the Climbing Image algorithm [50].

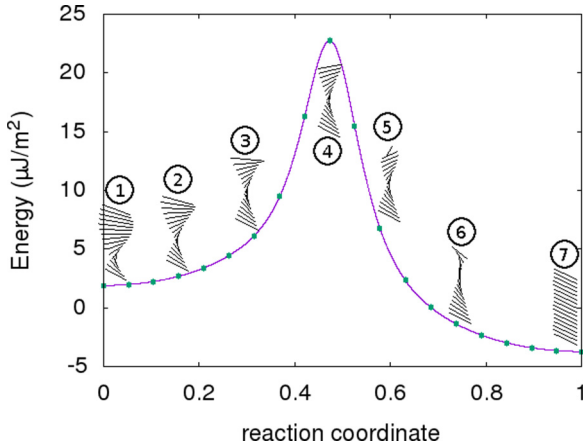


FIG. 2. Energy per unit area along the MEP for the director slippage transition computed at  $U = 0.53$  V and  $r_W = 1.0$ . The filled circles correspond to the images of the system used in the GNEB calculation. The reaction coordinate is defined as the displacement along the path normalized by its total length.

**B. Director slippage transitions**

According to Ref. [34], under certain conditions the pitch transitions being solely governed by in-plane director fluctuations do not involve tilted configurations and the transition mechanism can be described as director slippage through the energy barriers formed by the surface potentials. In what follows, such transitions will be referred to as the director slippage transitions.

In our calculations, the left-handed helix [see Fig. 1(a)] and the nematic equilibrium structure [see Fig. 1(c)] are used as the initial and final states, respectively. The starting approximation for the path involves the in-plane helical structures with  $\theta = \pi/2$  assuming that the azimuthal angle,  $\phi_+$ , at the top substrate uniformly varies along the path approaching the untwisted state value equal to the twist angle at the bottom substrate  $\phi_- = 0$ . In what follows such an initial approximation of the MEPs will be called the *director slippage approximation*.

In Fig. 2, we present the energies of director configurations along the MEP computed at  $U = 0.53$  V and  $r_W \equiv W_\theta/W_\phi = 1.0$ . In addition, Fig. 2 shows the director structures for a set of the selected images (the total number of the computed images is 18) along the path. The first image is the metastable helical structure, whereas the last image is the stable nematic state. The fourth numbered image is the transition (saddle-point) state giving the energy that determines the energy barrier (activation energy) of the transition. The profiles of the azimuthal angle  $\phi$  for CLC structures shown in Fig. 2 are plotted in Fig. 3. Clearly, similar to the initial and final states, the profile for the transition state appears to be linear with the director at the top substrate oriented along the normal to the easy axis. By contrast, it turns out that the profiles of other states along the MEP demonstrate nonlinear behavior of the azimuthal angle evaluated as a function of  $z$ . Such profiles significantly differ from the Grandjean texture (1).

The director slippage scenario implies that, below the threshold voltage, tilted structures have no effect on unwinding of the helix and the corresponding MEPs. For the planar

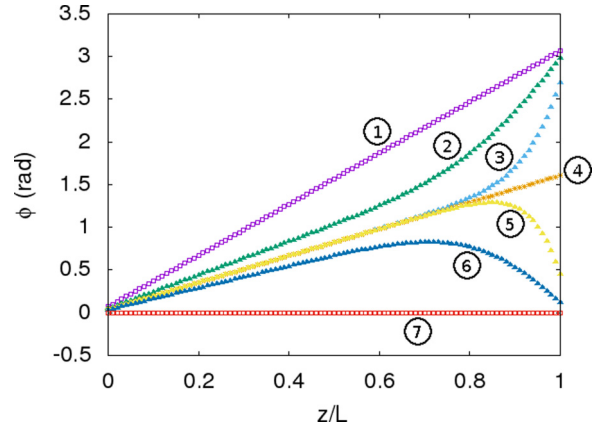


FIG. 3. Profiles of the azimuthal angle for each image in the MEP for the director slippage transition.

structures with  $\theta = \pi/2$ , the orientation dependent part of the energy (4) is independent of both the polar anchoring strength  $W_\theta$  and the applied voltage  $U$ . In particular, for the ideal helical structures (1), this energy is

$$F_0(\alpha, \beta) = \frac{K_2}{2L}(\beta - \beta_0) + \frac{W_\phi}{4}[2 - \cos(\beta + \alpha) - \cos(\beta - \alpha)], \tag{15}$$

where  $\beta = qL$  and  $\alpha = 2\phi_0$  gives the two-dimensional free energy surface. Part of this surface with the two minima representing the twisted ( $\beta \approx -\pi$ ) and unwound ( $\beta \approx 0$ ) structures under consideration is depicted in Fig. 4(a).

The energy along the path connecting the minima and passing through the saddle point [this path is shown as the red line in Fig. 4(a)] is plotted versus the twisting parameter  $\beta$  in Fig. 4(b). It can be readily found that the saddle-point state is the structure with  $\alpha = -\beta = \pi/2$  and the energy barrier can be estimated at about  $\Delta E = F_0(\pi/2, -\pi/2) - F_0(\pi, -3.07) \approx 22.6 \mu\text{J}/\text{m}^2$ . This estimate is close to  $W_\phi/2$ .

When using the minimum-energy paths method, a MEP evaluated at certain values of the anchoring ratio  $r_W$  and the applied voltage  $U$  gives the energy barrier  $\Delta E(r_W, U)$  computed as the difference between the energies of the transition (saddle-point) state and of the initial twisted state. The energy barrier map in the  $r_W$ - $U$  plane computed for the director slippage transitions is presented in Fig. 5. In agreement with the above discussion, below the critical voltage  $U_{th}$ , the director structure of the transition state is uniformly twisted and the energy barrier is independent of both the anchoring ratio  $r_W$  and the voltage  $U$  (for illustrative purposes, the low-voltage part of the map shown in Fig. 5 is truncated). In this low-voltage regime, the above analysis of the ideal helical structures and the MEP method give identical results for the value of the energy barrier.

As is seen from Fig. 5, above the threshold voltage  $U_{th}$  of the Fréedericksz transition, the energy barrier increases with the anchoring ratio  $r_W$  and, in general, is a nonmonotonic function of the applied voltage  $U$ . In this region, the planar states are unstable and all the structures involved in the transitions are deformed by the applied field. These are the tilted structures characterized by profound out-of-plane

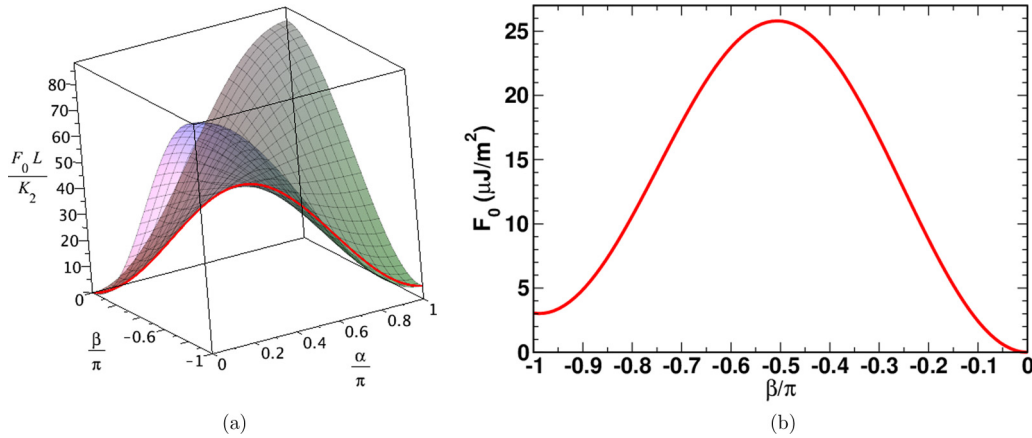


FIG. 4. (a) Free energy surface for the helical structures (1). (b) Energy along the path passing through the saddle point. The energy barrier is  $\Delta E \approx 22.6 \mu\text{J}/\text{m}^2$ .

director deviations. The MEPs above the critical voltage  $U_{th}$  will be discussed in Sec. III D.

**C. Anchoring breaking transitions**

In order to study an alternative scenario of the unwinding transition, we have used another starting approximation for the MEPs that involves the CLC structures where the uniform twist from  $\phi_- = 0$  to  $\phi_+$  is superimposed by the out-of-plane director deformation with the polar angle  $\theta$  varying from  $\theta_- = \pi/2$  to  $\theta_+$ . In this approximation, similar to the case of the director slippage transitions, the twist angle  $\phi_+$  along the path monotonically unwinds changing from  $-\pi$  to zero. By contrast, for the polar angle  $\theta_+$  at the top substrate, the initial decrease from  $\theta_+ = \pi/2$  to the value close to zero  $\theta_+ \approx 0$  that occurs in the first half of the path is followed by the increase in  $\theta_+$  that restores its initial value  $\theta_+ = \pi/2$  at the final state in the second half of the path. So, the initial guess for the MEP assumes that, for the transition state, the CLC director at the top substrate is nearly normal to the bounding surface. Such

a starting guess will be referred to as the *anchoring breaking approximation*.

Figure 6 presents the results for the energies of the CLC structures along the MEP computed at  $U = 0.53 \text{ V}$  and  $W_\theta/W_\phi = 1.25$  using the initial anchoring breaking approximation. Similar to Fig. 2, the first image is the metastable left-handed helical structure and the last image represents the stable untwisted state. The energy barrier is determined by the energy of the transition state corresponding to the fifth numbered image.

As is illustrated in Fig. 6, in the first half of the path, the region of pronounced out-of-plane deviation approaches the top boundary surface reaching the transition (saddle-point) structure with the director orientation close to the normal to the substrate ( $\theta \approx 0$ ). Such structure implies that the twisted structure unwinds via anchoring breaking that occurs at the upper substrate and such unwinding transition will be referred to as the anchoring breaking transition.

Note that, in contrast to the director slippage transition (see Fig. 2), there is a flattened region in the close vicinity of the maximum of the energy curve shown in Fig. 6. The reason is that, at  $\theta \approx 0$ , variations in the azimuthal angle  $\phi$  have negligible effect on the energy. On the other hand,

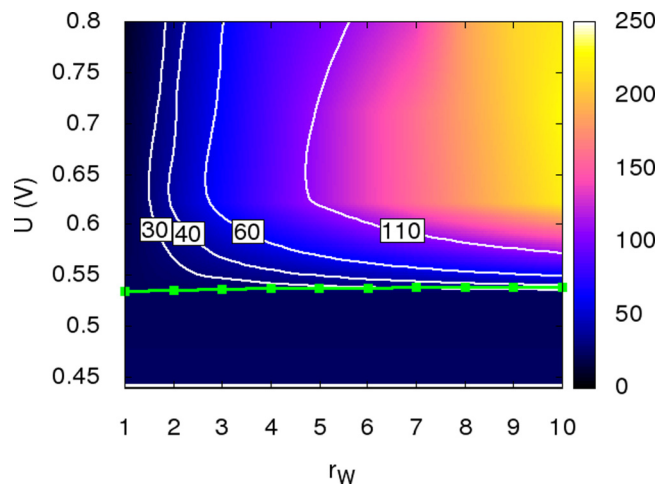


FIG. 5. Energy barrier map in the  $r_W$ - $U$  plane for the director slippage transitions. The green line with squares indicates the threshold voltage of the Fréedericksz transition  $U_{th}$  and the energy barrier scale is given in  $\mu\text{J}/\text{m}^2$ .

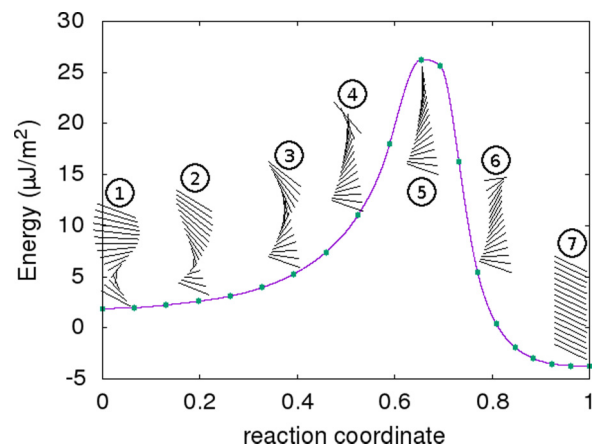


FIG. 6. Energy per unit area along the MEP for the anchoring breaking transition computed at  $U = 0.53 \text{ V}$  and  $r_W = 1.25$ .

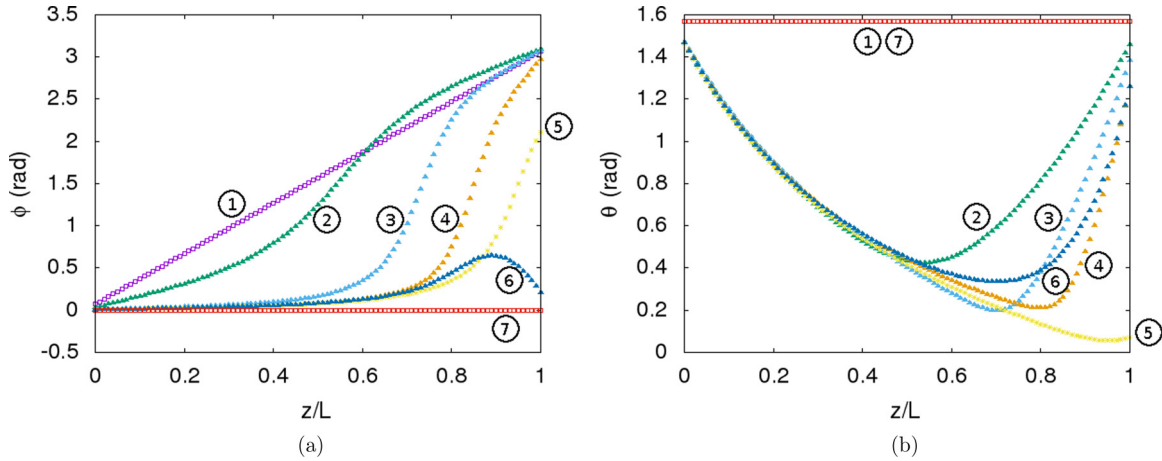


FIG. 7. Profiles of (a) the azimuthal and (b) the polar angles for each image in the MEP for the anchoring breaking transition.

these variations produce noticeable changes in the reaction coordinate which is the normalized sum of the angles,  $\theta$  and  $\phi$ , along the path.

The profiles of the azimuthal and the polar angles computed for the images of the anchoring breaking transition shown in Fig. 6 are presented in Figs. 7(a) and 7(b), respectively. It can be seen that, except for the initial and final states, all the profiles are nonlinear. The fifth curve for the polar angle of the transition state clearly shows homeotropic orientation of the director at the upper substrate with  $\theta_+ \approx 0$ .

In Fig. 8, we show the results for the energy barrier computed as a function of the anchoring ratio  $r_W$  and the voltage  $U$ . From the energy barrier map presented in Fig. 8, it can be inferred that the energy barrier is independent of  $r_W$  and  $U$  until the voltage exceeds its critical value  $U_c \approx 0.29$  V. So, at  $U < U_c$ , the anchoring breaking approximation produces the results identical to the director slippage transitions. For the voltages above  $U_c$ , the tilted CLC structures come into play and the anchoring strength  $W_\theta$  will affect the values of the energy barrier.

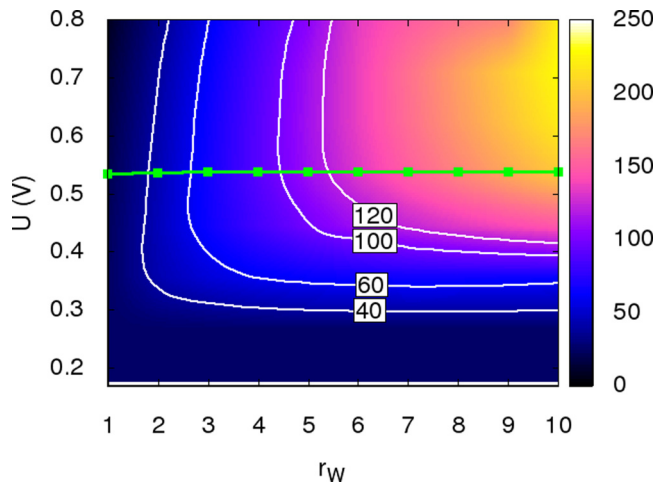


FIG. 8. Energy barrier map in the  $r_W$ - $U$  plane for the anchoring breaking transitions. The green line with squares indicates the threshold voltage of the Fréedericksz transition  $U_{th}$  and the energy barrier scale is given in  $\mu\text{J}/\text{m}^2$ .

**D. Comparison between two scenarios**

Below the threshold voltage  $U < U_{th}$ , dependence of the energy barrier on  $W_\theta$  originates from the tilted saddle-point structure representing the transition state. The corresponding out-of-plane deviations of the director can be quantitatively described by the minimum polar angle

$$\theta_{\min} = \min_z \theta(z) \tag{16}$$

evaluated for the transition state of a MEP. The smaller the value of  $\theta_{\min}$  is the more tilted the saddle-point state is.

The maps of the angle  $\theta_{\min}$  in the  $r_W$ - $U$  plane calculated using the director slippage and the anchoring breaking initial approximations are shown in Figs. 9(a) and 9(b), respectively. Referring to Fig. 9, it can be seen that, for the anchoring breaking transitions, a noticeable decrease in  $\theta_{\min}$  takes place when the voltage exceeds  $U_c$ , whereas, for the director slippage transitions, this happens in the close vicinity of the threshold voltage  $U_{th}$ . So, we arrive at the conclusion that the two mechanisms become essentially distinct at voltages higher than  $U_c$ .

In order to further emphasize the difference between the two scenarios, Fig. 10 presents the distribution of the ratio of the energy barriers in the  $r_W$ - $U$  plane. It can be seen that, at  $U > U_c$ , this ratio is an increasing function of  $r_W$  and, when the difference between the azimuthal and polar anchoring strengths is small with  $r_W \approx 1$ , the barriers are nearly equal.

It turns out that, even after the Fréedericksz transition takes place, the barriers of the MEPs may significantly differ. The maximum value of the barrier ratio is reached at large values of anchoring strength ratio in the voltage interval lying just above the threshold voltage. This is the interval where, according to Figs. 5 and 9, the effect of the saddle-point tilt for the director slippage scenario is much less pronounced as compared to the MEPs evaluated using the anchoring breaking initial approximation.

When the voltage further increases, the transition state director structures will be dominated by the field induced deformations. As is clearly demonstrated in Fig. 10, the result is that the two scenarios eventually merge into one and become indistinguishable at sufficient voltages above the Fréedericksz threshold.

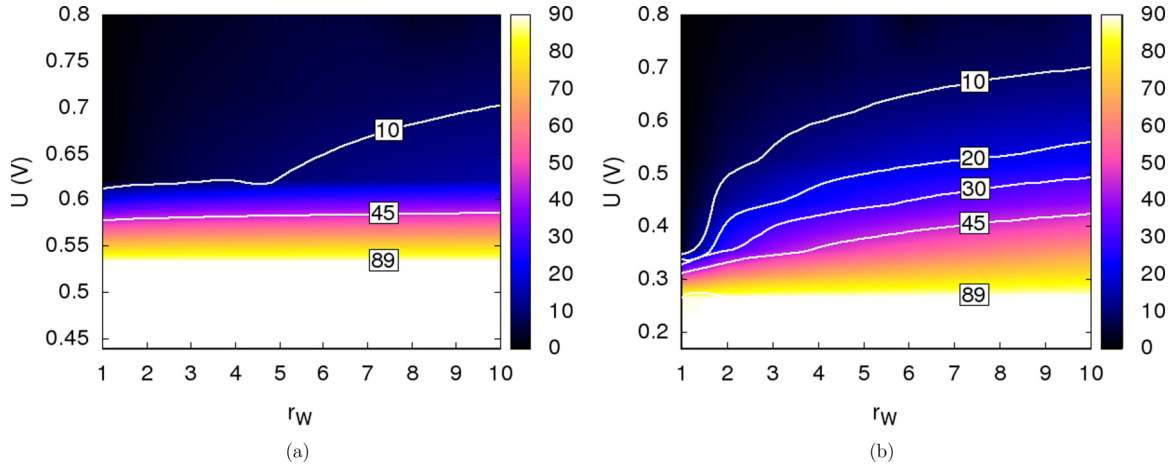


FIG. 9. Map of the minimum polar angle  $\theta_{\min} [\equiv \min_z \theta(z)]$  at the saddle point (transition state) for (a) the director slippage transition and (b) the anchoring breaking transition in the  $r_W$ - $U$  plane. For each contour line, digits in squares indicate the value of  $\theta_{\min}$  measured in degrees.

We have used the initial anchoring breaking approximation to compute the MEP in this high-voltage region ( $U = 0.64$  V) at the anchoring strength ratio  $r_W = 2$ . The results for the energies along the MEP and for the profiles of the azimuthal and polar angles are shown in Figs. 11 and 12, respectively. Interestingly, the transition state (the fifth numbered image and its profiles) of this MEP bears close resemblance to the one for the anchoring breaking transition (see Figs. 6 and 7). By contrast to the latter, the initial twisted and the final untwisted states (the first and the seventh images, respectively) of this transition reveal significant out-of-plane deformations induced by the electric field.

#### IV. CONCLUSION

In this paper, we have studied the minimum-energy paths for the unwinding transition in the chiral nematic liquid crystal cell. Such pathways connect the metastable CLC states, which are local minima of the multidimensional free energy surface, and the energy of the saddle point (transition state) of the paths gives the energy barrier separating the metastable states.

Therefore, the MEP and its saddle points characterize the mechanism (scenario) of the transition.

We have employed the GNEB method as a computational procedure to evaluate the MEPs. This method requires an initial guess for the path and various starting approximations can generally produce different MEPs. In our approach, this dependence of the MEPs on the starting approximation is exploited to examine two scenarios of the unwinding transition from the metastable left-handed CLC helix to the ground untwisted state. For this purpose, we have used the director slippage (see Sec. III B) and the anchoring breaking (see Sec. III C) approximations as the starting paths for the MEPs.

These MEPs and the energy barriers are calculated at various values of the voltage  $U$  applied across the CLC cell and the anchoring strength ratio  $r_W = W_\theta/W_\phi$ . For the director slippage scenario, orientational configuration of the transition state is found to remain planar until the voltage reaches the Fréedericksz threshold  $U_{th}$ . By contrast, in the saddle-point state of the MEPs representing the anchoring breaking

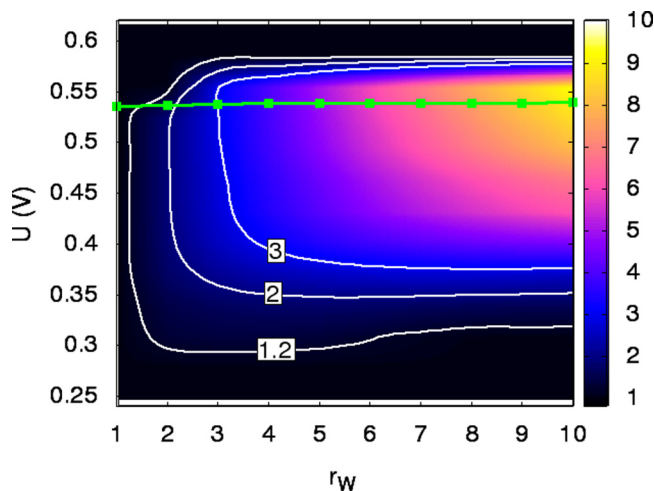


FIG. 10. Map of the ratio of the energy barriers for the anchoring breaking and the director slippage transitions in the  $r_W$ - $U$  plane.

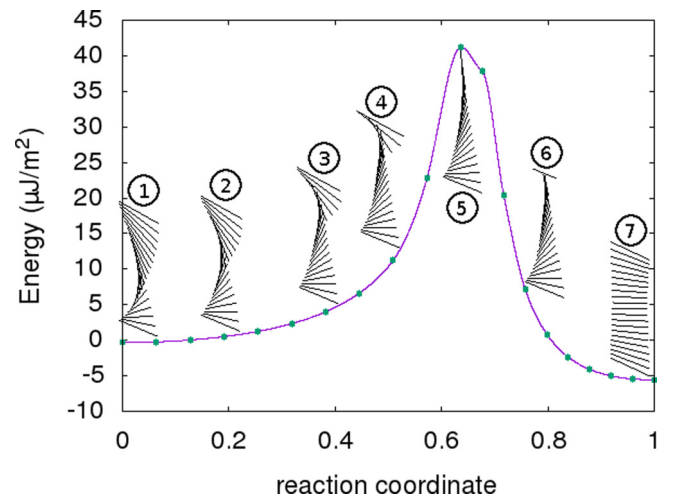


FIG. 11. Energy per unit area along the MEP for the transition above the Fréedericksz threshold computed at  $r_W = 2$  and  $U = 0.64$  V.

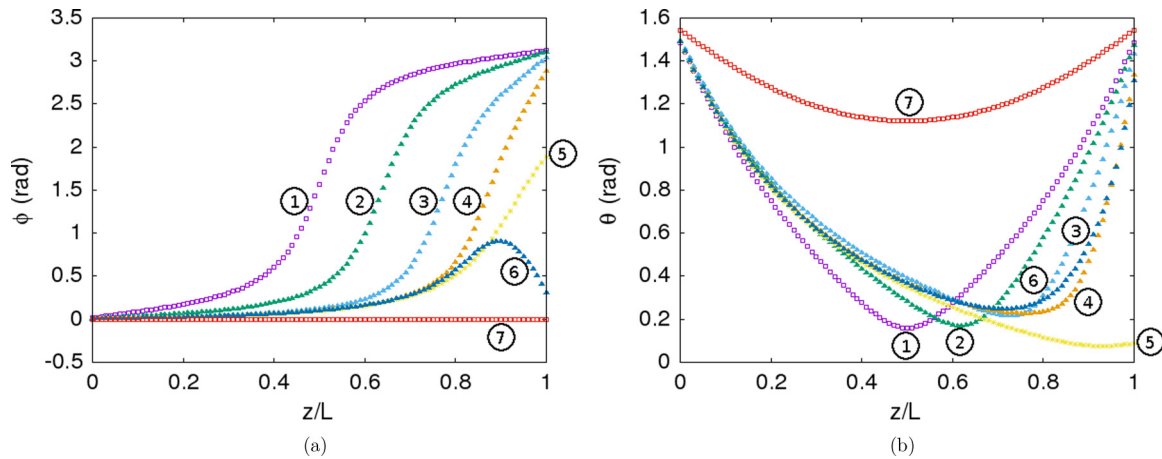


FIG. 12. Profiles of (a) the azimuthal and (b) the polar angles for the images along the MEP calculated above the Fréedericksz transition at  $r_W = 2$  and  $U = 0.64$  V.

scenario of the transition, out-of-plane deformations of the director structure are localized near the bounding surface chosen by the initial approximation. This scenario comes into play only when the voltage exceeds its critical value  $U_c < U_{th}$ .

At voltages above the Fréedericksz threshold  $U_{th}$ , both the initial metastable twisted state and the final untwisted state are deformed by the applied electric field. In this case, electrically induced deformations also affect the saddle-point state of the MEPs computed using the director slippage approximation. The result is that the difference between the two scenarios becomes negligible at sufficiently high voltages (see Fig. 10). Note that, in the low-voltage region where  $U < U_c$ , the director structure of the transition state is a planar Grandjean texture (1) and the MEPs, similar to the high-voltage regime, are indistinguishable.

Figure 10 also shows that, at  $U > U_c$ , the energy barrier ratio increases with the anchoring strength ratio  $r_W$  (and the polar anchoring strength  $W_\theta$ ) and, when the difference between the azimuthal and polar anchoring strengths is small with  $r_W \approx 1$ , the barriers are nearly equal. Figure 9 illustrates that, as opposed to the voltage, an increase in  $r_W$  reduces the maximal tilt angle of the saddle-point structure (this angle

is equal to  $\pi/2 - \theta_{min}$ ). Since the polar anchoring strength determines energy cost of out-of-plane deformations at the surface this result comes as no surprise.

Our results are limited to the one-dimensional case where the LC structures depend on one spatial variable. The three-dimensional case with the generalized anchoring conditions requires a more sophisticated analysis. This work is in progress and the results will be published elsewhere.

We conclude with the remark that the saddle-point states can also be found without knowledge of the final state using the minimum mode following the method recently suggested in Ref. [59]. This promising method, being more complicated than the GNEB method, allows discovering unexpected final states and the transition mechanisms.

#### ACKNOWLEDGMENTS

This work was supported by Russian Foundation of Basic Research under Grant No. 18-02-00267 and by the Foundation for Advancement of Theoretical Physics and Mathematics BASIS under Grant No. 19-1-1-12-1.

- 
- [1] P. G. de Gennes and J. Prost, *The Physics of Liquid Crystals* (Clarendon, Oxford, 1993), p. 596.
- [2] P. Oswald and P. Pieranski, *Nematic and Cholesteric Liquid Crystals: Concepts and Physical Properties Illustrated by Experiments*, The Liquid Crystals Book Series (Taylor & Francis, London, 2005), p. 618.
- [3] D.-K. Yang and S.-T. Wu, *Fundamentals of Liquid Crystal Devices*, Series in Display Technology (Wiley, New York, 2006), p. 378.
- [4] S. Obayya, M. F. O. Hameed, and N. F. F. Areed, *Computational Liquid Crystal Photonics: Fundamentals, Modelling and Applications* (Wiley, New York, 2016), p. 264.
- [5] H. K. Bisoyi, T. J. Bunning, and Q. Li, Stimuli-driven control of the helical axis of self-organized soft helical superstructures, *Adv. Mater.* **30**, 1706512 (2018).
- [6] R. S. Zola and Q. Li, Stimuli-directed helical axis switching in chiral liquid crystal nanostructures, in *Functional Organic and Hybrid Nanostructured Materials* (Wiley, New York, 2018), Chap. 8, pp. 307–357.
- [7] A. Ryabchun and A. Bobrovsky, Cholesteric liquid crystal materials for tunable diffractive optics, *Adv. Opt. Mater.* **6**, 1800335 (2018).
- [8] R. Balamurugan and J.-H. Liu, A review of the fabrication of photonic band gap materials based on cholesteric liquid crystals, *Reactive Funct. Polym.* **105**, 9 (2016).
- [9] F. C. Frank, On the theory of liquid crystals, *Discuss. Faraday Soc.* **25**, 19 (1958).
- [10] C. W. Oseen, The theory of liquid crystals, *Trans. Faraday Soc.* **29**, 883 (1933).

- [11] V. Vinogradov, A. Khizhnyak, L. Kutulya, Y. Reznikov, and V. Reshetnyak, Photoinduced change of cholesteric LC-pitch, *Mol. Cryst. Liq. Cryst.* **192**, 273 (1990).
- [12] R. A. van Delden, T. Mecca, C. Rosini, and B. L. Feringa, A chiroptical molecular switch with distinct chiral and photochromic entities and its application in optical switching of a cholesteric liquid crystal, *Chemistry: A Eur. J.* **10**, 61 (2004).
- [13] R. Eelkema, Photo-responsive doped cholesteric liquid crystals, *Liq. Cryst.* **38**, 1641 (2011).
- [14] N. Katsonis, E. Lacaze, and A. Ferrarini, Controlling chirality with helix inversion in cholesteric liquid crystals, *J. Mater. Chem.* **22**, 7088 (2012).
- [15] T. N. Orlova, R. I. Iegorov, and A. D. Kiselev, Light-induced pitch transitions in photosensitive cholesteric liquid crystals: Effects of anchoring energy, *Phys. Rev. E* **89**, 012503 (2014).
- [16] Z.-G. Zheng, L. Yannian, H. K. Bisoyi, L. Wang, T. J. Bunning, and Q. Li, Three-dimensional control of the helical axis of a chiral nematic liquid crystal by light, *Nature (London)* **531**, 352 (2016).
- [17] H. K. Bisoyi and Q. Li, Light-directed dynamic chirality inversion in functional self-organized helical superstructures, *Angew. Chem., Int. Ed. Engl.* **55**, 2994 (2016).
- [18] H. Huang, T. Orlova, B. Matt, and N. Katsonis, Long-lived supramolecular helices promoted by fluorinated photoswitches, *Macromol. Rapid Commun.* **39**, 1700387 (2018).
- [19] S. Kurihara, T. Kanda, T. Nagase, and T. Nonaka, Photochemical color switching behavior of induced cholesteric liquid crystals for polarizer free liquid crystalline devices, *Appl. Phys. Lett.* **73**, 2081 (1998).
- [20] T. J. White, A. S. Freer, N. V. Tabiryan, and T. J. Bunning, Photoinduced broadening of cholesteric liquid crystal reflectors, *J. Appl. Phys.* **107**, 073110 (2010).
- [21] T. Kosa, L. Sukhomlinova, L. Su, B. Taheri, T. J. White, and T. J. Bunning, Light-induced liquid crystallinity, *Nature (London)* **485**, 347 (2012).
- [22] J. P. Vernon, A. D. Zhao, R. Vergara, H. Song, V. P. Tondiglia, T. J. White, N. V. Tabiryan, and T. J. Bunning, Photostimulated control of laser transmission through photoresponsive cholesteric liquid crystals, *Opt. Express* **21**, 1645 (2013).
- [23] D. W. Berreman and W. R. Heffner, New bistable liquid-crystal twist cell, *J. Appl. Phys.* **52**, 3032 (1981).
- [24] R. D. Kamien and J. V. Selinger, Order and frustration in chiral liquid crystals, *J. Phys. Condens. Matter* **13**, R1 (2000).
- [25] N. J. Mottram and S. J. Hogan, Multiple solutions in twisted nematic liquid crystal layers, *Continuum Mech. Thermodyn.* **9**, 213 (1997).
- [26] M. Robinson, C. Luo, P. E. Farrell, R. Erban, and A. Majumdar, From molecular to continuum modelling of bistable liquid crystal devices, *Liq. Cryst.* **44**, 2267 (2017).
- [27] H. Zink and V. A. Belyakov, Temperature hysteresis of the change in the cholesteric pitch and surface anchoring in thin planar layers, *JETP* **85**, 285 (1997).
- [28] J. V. Gandhi, X.-D. Mi, and D.-K. Yang, Effect of surface alignment layers on the configurational transitions in cholesteric liquid crystals, *Phys. Rev. E* **57**, 6761 (1998).
- [29] H. Zink and V. A. Belyakov, Studies of the temperature pitch variations in planar cholesteric layer and surface anchoring, *Mol. Cryst. Liq. Cryst.* **329**, 457 (1999).
- [30] H. G. Yoon, N. W. Roberts, and H. F. Gleeson, An experimental investigation of discrete changes in pitch in a thin, planar chiral nematic device, *Liq. Cryst.* **33**, 503 (2006).
- [31] V. A. Belyakov and E. I. Kats, Surface coupling and temperature variations of pitch in thin cholesteric layers, *JETP* **91**, 488 (2000).
- [32] V. A. Belyakov, P. Oswald, and E. I. Kats, Temperature pitch variations in planar cholesteric layers: The role of fluctuations and surface anchoring, *JETP* **96**, 915 (2003).
- [33] S. P. Palto, On mechanisms of the helix pitch variation in a thin cholesteric layer confined between two surfaces, *JETP* **94**, 260 (2002).
- [34] A. D. Kiselev and T. J. Sluckin, Twist of cholesteric liquid crystals cells: Stability of helical structures and anchoring energy effects, *Phys. Rev. E* **71**, 031704 (2005).
- [35] G. McKay, Bistable surface anchoring and hysteresis of pitch jumps in a planar cholesteric liquid crystal, *Eur. Phys. J. E* **35**, 74 (2012).
- [36] I. Lelidis, G. Barbero, and A. L. Alexe-Ionescu, Cholesteric pitch transitions induced by mechanical strain, *Phys. Rev. E* **87**, 022503 (2013).
- [37] G. Barbero, W. Zheng, and B. Zappone, Twist transitions and force generation in cholesteric liquid crystal films, *J. Mol. Liq.* **267**, 242 (2018), Special Issue Dedicated to the Memory of Professor Y. Reznikov.
- [38] C.-K. Liu, M.-C. Tsai, S. M. Morris, C.-Y. Chiu, C.-C. Chen, and K.-T. Cheng, Dynamics of pitch change in chiral azobenzene-doped liquid crystals, *J. Mol. Liq.* **263**, 406 (2018).
- [39] P. Oswald, Measurement with a rotating magnetic field of the surface viscosity of a nematic liquid crystal, *Europhys. Lett.* **100**, 26001 (2012).
- [40] A. Martinez and I. I. Smalyukh, Light-driven dynamic Archimedes spirals and periodic oscillatory patterns of topological solitons in anisotropic soft matter, *Opt. Express* **23**, 4591 (2015).
- [41] R. F. de Souza, E. K. Lenzi, R. T. de Souza, L. R. Evangelista, Q. Li, and R. S. Zola, Surface induced twist in nematic and chiral nematic liquid crystals: Stick-slip-like and constrained motion, *Soft Matter* **14**, 2084 (2018).
- [42] R. B. Meyer, Effects of electric and magnetic fields on the structure of cholesteric liquid crystals, *Appl. Phys. Lett.* **12**, 281 (1968).
- [43] M. E. Becker, J. Nehring, and T. J. Scheffer, Theory of twisted nematic layers with weak boundary coupling, *J. Appl. Phys.* **57**, 4539 (1985).
- [44] P. Schiller, Equilibrium structures of planar nematic and cholesteric films in electric fields, *Phase Transitions* **29**, 59 (1990).
- [45] H. Hirning, W. Funk, H.-R. Trebin, M. Schmidt, and H. Schmiedel, Threshold behavior and electro-optical properties of twisted nematics layers with weak anchoring in the tilt and twist angle, *J. Appl. Phys.* **70**, 4211 (1991).
- [46] I. I. Smalyukh, B. I. Senyuk, P. Palffy-Muhoray, O. D. Lavrentovich, H. Huang, E. C. Gartland, V. H. Bodnar, T. Kosa, and B. Taheri, Electric-field-induced nematic-cholesteric transition and three-dimensional director structures in homeotropic cells, *Phys. Rev. E* **72**, 061707 (2005).
- [47] S. S. Choi, S. M. Morris, W. T. S. Huck, and H. J. Coles, Electrically tuneable liquid crystal photonic bandgaps, *Adv. Mater.* **21**, 3915 (2009).

- [48] A. Yu. Val'kov, E. V. Aksenova, and V. P. Romanov, First-order and continuous Fréedericksz transitions in cholesteric liquid crystals, *Phys. Rev. E* **87**, 022508 (2013).
- [49] H. Kusumaatmaja and A. Majumdar, Free energy pathways of a multistable liquid crystal device, *Soft Matter* **11**, 4809 (2015).
- [50] P. F. Bessarab, V. M. Uzdin, and H. Jónsson, Method for finding mechanism and activation energy of magnetic transitions, applied to skyrmion and antivortex annihilation, *Comput. Phys. Commun.* **196**, 335 (2015).
- [51] A. V. Ivanov, P. F. Bessarab, E. V. Aksenova, V. P. Romanov, and V. M. Uzdin, Energy surface and minimum energy paths for Fréedericksz transitions in bistable cholesteric liquid crystals, *Phys. Rev. E* **93**, 042708 (2016).
- [52] P. Hänggi, P. Talkner, and M. Borkovec, Reaction-rate theory: Fifty years after Kramers, *Rev. Mod. Phys.* **62**, 251 (1990).
- [53] W. T. Coffey, D. A. Garanin, and D. J. McCarthy, Crossover formulas in the Kramers theory of thermally activated escape rates: Application to spin systems, in *Advances in Chemical Physics* (Wiley, New York, 2007), Chap. 5, pp. 483–765.
- [54] P. Goldbart and P. Ao, Intrinsic Torsional Viscosity of Nematic Liquid Crystals, *Phys. Rev. Lett.* **64**, 910 (1990).
- [55] P. M. Goldbart and P. Ao, Intrinsic torsional viscosity in a narrow tube of nematic liquid crystal, *Mol. Cryst. Liq. Cryst.* **198**, 455 (1991).
- [56] A. Rapini and M. Papoular, Distorsion d'une lamelle nématique sous champ magnétique conditions d'ancrage aux parois, *J. Phys. Colloq.* **30**, C4-54 (1969).
- [57] A. Bogi and S. Faetti, Elastic, dielectric and optical constants of 4'-pentyl-4-cyanobiphenyl, *Liq. Cryst.* **28**, 729 (2001).
- [58] H. Jónsson, G. Mills, and K. W. Jacobsen, Nudged elastic band method for finding minimum energy paths of transitions, in *Classical and Quantum Dynamics in Condensed Phase Simulations*, edited by B. J. Berne, G. Ciccotti, and D. F. Coker (World Scientific, Singapore, 1998).
- [59] G. P. Müller, P. F. Bessarab, S. M. Vlasov, F. Lux, N. S. Kiselev, S. Blügel, V. M. Uzdin, and H. Jónsson, Duplication, Collapse, and Escape of Magnetic Skyrmions Revealed Using a Systematic Saddle Point Search Method, *Phys. Rev. Lett.* **121**, 197202 (2018).